Journal of Southeast University (English Edition) Vol. 40, No. 3, pp. 257 - 265 Sept. 2024 ISSN 1003—7985

Design and evaluation of UHPP steel bridge deck pavement for high-temperature and rainy regions

Qian Zhendong[1] Zhang Shaojin[2] Min Yitong[1] Zhao Xinyuan[1]

([1]Intelligent Transportation System Research Center, Southeast University, Nanjing 211189, China)

([2]College of Architectural Science and Engineering, Yangzhou University, Yangzhou 510000, China)

Abstract: To enhance the serviceability of steel bridge deck pavement (SBDP) in high-temperature and rainy regions, a concept of rigid bottom and flexible top was summarized using engineering practices, which led to the proposal of a three-layer ultra-high-performance pavement (UHPP). The high-temperature rutting resistance and wet-weather skid resistance of UHPP were evaluated through composite structure tests. The internal temperature distribution within the pavement under typical high-temperature conditions was analyzed using a temperature field model. Additionally, a temperature-stress coupling model was employed to investigate the key load positions and stress response characteristics of the UHPP. The results indicate that compared with the traditional guss asphalt + stone mastic asphalt structure, the dynamic stability of the UHPP composite structure can be improved by up to 20.4%. Even under cyclic loading, UHPP still exhibits superior surface skid resistance compared to two traditional SBDPs. The thickness composition of UHPP significantly impacts its rutting resistance and skid resistance. UHPP exhibits relatively low tensile stress but higher shear stress levels, with the highest shear stress occurring between the UHPP and the steel plate. This suggests that the potential risk of damage for UHPP primarily lies within the interlayer of the pavement. Based on engineering examples, introducing interlayer gravel and optimizing the amount of bonding layer are advised to ensure that UHPP possesses sufficient interlayer shear resistance.

Key words: steel bridge deck pavement (SBDP); high-temperature environment; rainy weather; rigid bottom and flexible top; temperature field; composite structure

DOI: 10.3969/j.issn.1003-7985.2024.03.005

The southern regions of China are characterized by high temperatures, frequent rainfall, and heavy traffic[1]. Thus, the serviceability of steel bridge deck pavement (SBDP) in the area has been significantly weakened by the persistent occurrence of early-stage deterioration and insufficient antiskid performance[2-3].

Traditional SBDP includes epoxy asphalt (EA) + EA for rigid systems and guss asphalt (GA) + stone mastic asphalt (SMA) for flexible systems. EA + EA employs thermosetting epoxy asphalt, which results in an SBDP with high stiffness and strength. Hence, it is considered a rigid system. However, it often relies on continuous dense-graded designs, potentially resulting in relatively inadequate antiskid resistance. Thus, researchers have experimented with creating porous EA mixtures through variations in gradation and asphalt-aggregate ratios to mitigate the issue of insufficient skid resistance[4]. This type of mixture possesses increased surface texture depth, partially addressing the problem of antiskid resistance. Nonetheless, the porosity design can reduce the resistance to cracking of the mixture, thus limiting its application to long-span flexible steel bridges[5].

In GA + SMA, an almost zero void content dense-graded asphalt mixture is employed as the lower layer, and SMA containing an abundance of surface void structures is used as the upper layer. This combination results in satisfactory skid resistance. However, as both asphalts used in GA + SMA are thermoplastic materials, the high-temperature performance of the SBDP is relatively lacking[6]. Thus, researchers have sought to optimize and improve the high-temperature performance of GA + SMA from various aspects, such as the application of maximum nominal aggregate size, pavement layer thickness combinations, and types of polymer asphalt modifiers[7-8]. Although these studies aimed to unlock the full potential performance of GA + SMA, they have not entirely resolved the issue of thermoplastic materials being susceptible to deformation under high-temperature conditions.

Considering that maximum tensile stresses typically occur at the surface of the upper layer of SBDP, the lower layer must provide stable support to delay the development of rutting[9]. Research indicates that compared with flexible materials such as SMA and GA, rigid materials like EA and polyurethane-based mixtures exhibit a linear shrinkage coefficient that is relatively closer to that of steel bridge decks. When used as the lower pavement layer, rigid materials' strong bonding capabilities also signif-

Received 2023-11-10, **Revised** 2024-03-15.

Biography: Qian Zhendong (1969—), female, doctor, professor, qianzd@seu.edu.cn.

Foundation items: The National Natural Science Foundation of China (No. 51878167), the Postgraduate Research and Practice Innovation Program of Jiangsu Province (No. KYCX23_0300).

Citation: Qian Zhendong, Zhang Shaojin, Min Yitong, et al. Design and evaluation of UHPP steel bridge deck pavement for high-temperature and rainy regions[J]. Journal of Southeast University (English Edition), 2024, 40(3): 257 - 265. DOI: 10.3969/j.issn.1003-7985.2024.03.005.

icantly reduce the occurrence of distress between pavement layers, thereby mitigating moisture-induced corrosion of steel bridge structures in humid regions[10].

In recent years, the EA + SMA system, designed with a "rigid below, flexible above" approach, has been successfully applied to large-span steel bridge deck paving projects in China, such as the Wuxue Yangtze River Bridge and the Jiujiang Yangtze River Bridge. This system utilizes dense-graded rigid material EA mixtures as the lower pavement layer to isolate moisture intrusion and disperse vehicle loads and bridge bending stresses. Flexible SMA is employed as the upper pavement layer to provide vehicles with a rough yet smooth driving surface. During the operation of such SBDPs, only the upper SMA layer requires milling, replacement, or repair as necessary.

In high-temperature and rainy regions, SBDP must not only possess excellent high-temperature deformation resistance but also maintain sufficient surface void structure to ensure safe driving during rainy weather. Given these requirements and the rigid bottom and flexible top (RBFT) design concept, this paper proposes an SBDP solution, denoted as ultra-high-performance pavement (UHPP).

1 Design and Composition of UHPP

The RBFT concept serves two primary purposes. First, it utilizes materials with excellent crack resistance for the lower pavement layer to counteract the bending moments caused by the flexible steel bridge deck. Second, the upper pavement layer is constructed using more flexible and resilient materials, aiming to manage surface tensile stresses effectively and reduce cracking from top to bottom. The typical approach to implementing these two purposes involves using materials such as epoxy resin or polyurethane in the lower pavement layer. These materials undergo chemical reactions, forming a high-modulus three-dimensional network that effectively enhances pavement rigidity. For the upper pavement layer, flexibility can be improved using various methods, including increasing pavement thickness, adding high-elasticity modifiers, or incorporating fiber materials.

In the context of SBDP in high-temperature and rainy regions, four key requirements must be met for the RBFT concept:

1) The SBDP should be designed with two or more layers. The lower layer, with excellent crack resistance, serves as the base, whereas the upper layer is designed as a flexible wearing or antiskid layer. Given the significant modulus difference between the upper and lower layers, an intermediate transition layer may be introduced to improve the mechanical response of the SBDP.

2) The lower layer must possess better crack resistance compared with the upper layer. The use of thermosetting or inorganic adhesive materials is recommended to delay cracking propagation from top to bottom.

3) The upper layer should possess exceptional antiskid performance and sufficient surface texture.

4) To avoid significant stress concentration, the modulus of the intermediate transition layer should fall between that of the lower and upper layers, resulting from excessive deformation differences between these pavement layers.

On the basis of these requirements, this paper introduces UHPP SBDP. The SBDP comprises three primary layers arranged from bottom to top: the connecting layer, the structural layer, and the wearing layer. Modified emulsified asphalt is employed as the adhesive layer between these primary layers, as illustrated in Fig. 1.

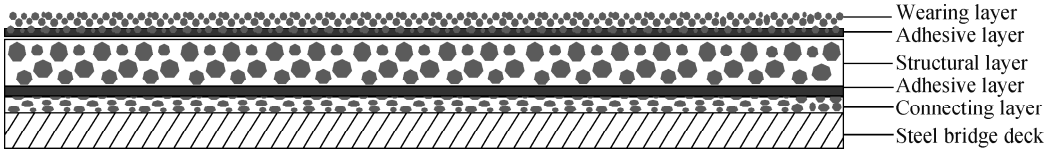

Fig. 1 UHPP SBDP

The connecting layer, known as UHPP-C, primarily protects the steel bridge deck from corrosion. Comprising epoxy resin and gravel with a particle size of 2.36 to 4.75 mm, this layer provides significantly higher bonding strength than asphalt materials. Its deformation capacity closely aligns with that of steel bridge decks, ensuring a secure bond.

The structural layer, designated as UHPP-S, is constructed using a polymer-modified asphalt mixture reinforced with basalt fibers. The reinforcing effect of basalt fibers effectively mitigates deformation and stress concentration resulting from steel bridge deck deflection and vehicle loads.

The protruding gravels on the surface of UHPP-C form a robust interlock with UHPP-S. An adhesive layer is positioned between UHPP-C and UHPP-S to disperse stresses and enhance interlayer bonding.

The wearing layer, known as UHPP-D, utilizes hard and wear-resistant diabase as the aggregate. This layer employs open gradation to improve skid resistance. A sufficient amount of modified emulsified asphalt is applied on top of UHPP-D, allowing it to penetrate the top of UHPP-S, forming a dense, waterproof adhesive layer.

UHPP-C and UHPP-S predominantly handle load-bear-

ing, whereas UHPP-D and the adhesive layer collectively provide drainage and antiskid functions for the entire pavement system. Even if the void structure in UHPP-D is compromised, it still maintains sufficient surface texture depth.

Performance test results for UHPP-C are shown in Table 1, whereas those for UHPP-S and UHPP-D are presented in Table 2.

Table 1 Main performance test results of UHPP-C

Pavement layer	Gradation type	Bonding strength to steel (60 ℃)/MPa	Tensile strength (25 ℃)/MPa	Bonding strength to UHPP-S (25 ℃)/MPa	Coefficient of linear contraction/10^{-5}
UHPP-C	Suspension dense	4.44	13.5	1.6	1.61

Table 2 Main performance test results of UHPP-S and UHPP-D

Pavement layer	Gradation type	Void/%	Dynamic stability (60 ℃)/(times · mm^{-1})	Ultimate tensile strain/10^{-6}	TSR/%
UHPP-S	Skeleton dense	3 to 4	6 570	3 539	≥90
UHPP-D	Open	17 to 25	4 160		≥92

2 Experimental Plan

2.1 Composite structure performance

In this section, a rutting test under a high temperature and an antiskid test during rainy weather on composite structure specimens were employed to evaluate the crucial performance characteristics of UHPP.

2.1.1 Materials

The performances of the raw materials involved in this section were tested following the Chinese standard JTG E20—2011. The performance test results of the binders used in UHPP-C, UHPP-S, and UHPP-D are shown in Tables 3-5, respectively. The performance test results of basalt fibers contained in UHPP-S are shown in Table 6. Herein, 4-cm EA + 4-cm EA and 4-cm GA + 4-cm SMA were selected as the control group, and their performance test results met the relevant requirements of the Chinese standard JTG/T 3364-02—2019. The gradation results of various types of mixtures are shown in Fig. 2.

Table 3 Performance testing results of the binder used in UHPP-C

Item	Adhesion to steel (25 ℃)/MPa	Compression strength (23 ℃)/MPa	Tensile strength (23 ℃)/MPa	Elongation rate (23 ℃)/MPa	Water absorption rate/%
Epoxy resin	6.4	49	15	18	0.03

Table 4 Performance testing results of the binder used in UHPP-S

Item	Penetration (25 ℃)/0.1 mm	Ductility (5 ℃)/cm	Softening point/℃	Dynamic viscosity (135 ℃)/(Pa · s)	Elastic recovery (25 ℃)
Modified asphalt	44	37	91.5	2.8	97

Table 5 Performance testing results of the binder used in UHPP-D

Item	Remaining/%	Viscosity $C_{25,3}$	Storage (24 h)/%	Evaporation residue			
				Penetration (25 ℃)/0.1 mm	Solubility/%	Ductility (5 ℃)/cm	Residual/%
Emulsified asphalt	0.03	22	0.6	67	97.9	33	71

Table 6 Performance testing results of the basalt fiber used in UHPP-S

Item	Filament diameter/μm	Nominal length/mm	Fracture strength/MPa	Elongation at break/%	Oil absorption rate/%
Basalt fiber	17.4	3.1	2 200	2.3	51.3

The optimum bitumen content of the mixtures described in this section was designed using the Marshall method. The bitumen contents were 5.8% for UHPP-S, 5.3% for UHPP-D, 6.3% for SMA, 7.8% for GA, and 6.6% for EA.

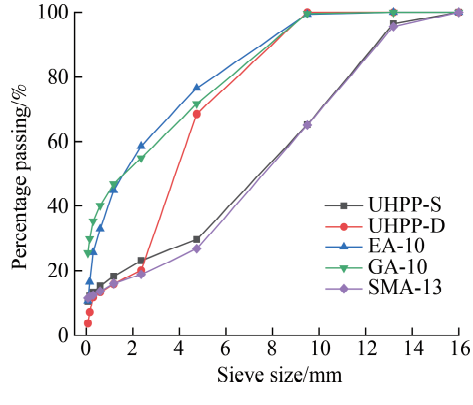

Fig. 2 Grading composition of mixtures

2.1.2 Rutting test under high temperature

The composite structure specimens were formed sequentially from bottom to top using a wheel-rolling machine. Considering the service temperature, the high-temperature rutting test temperature was set to 70 ℃ and the test load was set to 0.7 MPa. Referring to SBDP in China, the total pavement thickness was chosen as 80 mm[11]. The main function of UHPP-C was to improve the resistance to the bending moment of the steel bridge deck. Its thickness should not be too small. Therefore, referring to existing engineering applications[9], the thicknesses of UHPP composite structure specimens are shown in Table 7.

Table 7 Thickness of UHPP layers cm

Layer name	Group 1	Group 2	Group 3
UHPP-D	2	1.5	1
UHPP-S	5	5.5	6
UHPP-C	1	1	1

2.1.3 Antiskid test during rainy weather

To comprehensively evaluate the drainage performance of UHPP, the composite structure after the rutting test was segmented into 200 mm × 50 mm wide specimens. The segmentation was done along the paths of wheel load traces. The prefix "W" designates specimens that underwent the rutting test. Similarly, another set of composite structures was prepared using the same procedure and cut into identical samples. Sealant wax was applied to the side surfaces of the specimens along the wider edges, ensuring that water could only exit from the longer edges.

To simulate typical rainfall conditions in high-temperature and rainy regions, a custom-designed rain simulator (see Fig. 3) was employed to spray water over the specimens. Thereafter, a pendulum-type deflection meter measured the surface deflection of the specimens under varying rainfall intensities. The friction coefficient was then calculated by

$$\mu = \frac{B_{PN}}{100} \tag{1}$$

where μ refers to the friction coefficient and B_{PN} refers to the pendulum value from the national standard (JTG 3450—2019).

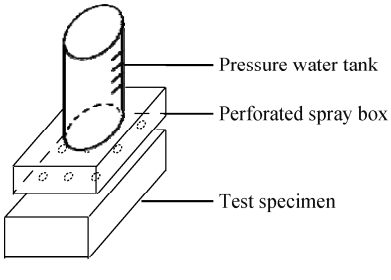

Fig. 3 Custom-designed rain simulator

2.2 Finite element simulation

The box girder model established in this section comprises two transverse diaphragms and the SBDP, involving a total of 49 920 finite elements. The SBDP utilized eight-node linear hexahedral elements. The geometric parameters were derived from a newly constructed large-span steel bridge in China, and the critical parameters used for this model can be found in Fig. 4. In the model, the U-rib cross-section has an opening width of 300 mm, a height of 280 mm, and a thickness of 8 mm. The thickness of the transverse diaphragm is 8 mm, and the spacing between adjacent transverse diaphragms is 300 mm. The thickness of the steel bridge deck is 14 mm.

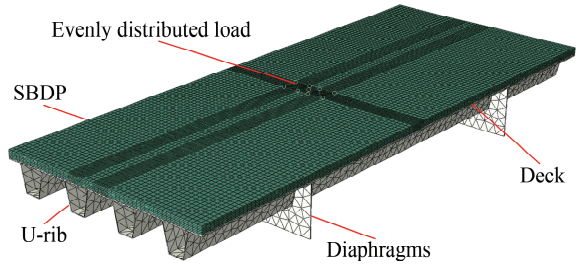

Fig. 4 Model established in Abaqus

2.2.1 Temperature field model

The temperature field model's boundary conditions were defined by controlling three parameters related to external conditions: the heat exchange coefficient with the surroundings (B), daily solar radiation ($Q(t)$), and daily ambient air temperature variations ($T(t)$). These boundary conditions are defined as follows.

1) The heat exchange between SBDP and its surroundings occurs primarily through two mechanisms: solar radiation from the sun, denoted as B_s, and convective heat exchange between the pavement and the surrounding ambient air temperature variations, denoted as B_k. Therefore, the calculation of the external heat exchange coefficient (B) is expressed by

$$B = B_s + B_k \tag{2}$$

$$B_s = C_p K_p \tag{3}$$

$$B_k = 3.7v + 9.4 \tag{4}$$

where C_p is the material constant, which is 3.46 for asphalt mixture; K_p is the temperature coefficient; v is the ambient wind speed, $v = 2.5$ m/s.

2) Based on regional meteorological data and using daily maximum and minimum temperatures as input, the following computational model is fitted:

$$Q(t) = \begin{cases} 0 & t \in \left[0, 12 - \dfrac{c}{2}\right) \\ Q_0 \cos[mw(t-12)] & t \in \left[12 - \dfrac{c}{2}, 12 + \dfrac{c}{2}\right] \\ 0 & t \in \left(12 + \dfrac{c}{2}, 24\right] \end{cases} \tag{5}$$

where Q_0 represents the maximum radiation from the sun at noon on a single day, $Q_0 = 0.131 m Q_s$; m is the atmos-

pheric optical parameter, and $m = 12/c$; Q_s represents the daily total solar radiation, $Q_s = 28.3 \times 10^6$ J/m^2; c is the daily effective sunshine time, and $c = 12$ h; w represents the angular frequency, and $w = 2\pi/24$.

3) Ambient air temperature is also one of the direct factors influencing the temperature of SBDP. In this study, a combination of sine functions is employed to describe this temperature variation process as follows:

$$T(t) = \frac{T_{max} + T_{min}}{2} + \frac{T_{max} - T_{min}}{2}\{0.96\sin[\omega(t - t_0)] + 0.146\sin[2\omega(t - t_0)]\} \quad (6)$$

where T_{max} represents the daily highest temperature; T_{min} represents the daily lowest temperature; and t_0 represents the initial time.

The 24-h temperature data of Guangdong was chosen as the environmental variable[12], as shown in Fig. 5. The thermodynamic parameters used in the model are shown in Table 8. In the model, the solar radiation absorptivity of the environment was set to 0.9, and the material emissivity coefficient was set to 0.81.

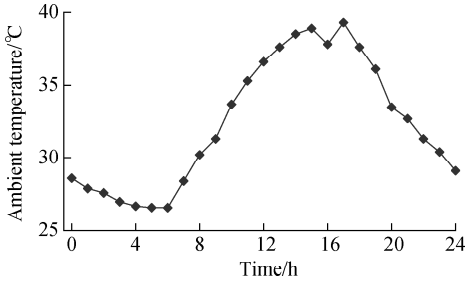

Fig. 5 24-h temperature data used in the model

Table 8 Thermodynamic parameters of SBDP

Item	Thermal conductivity/ (W · (m · K)$^{-1}$)	Density/ (kg · m^{-3})	Heat capacity/ (J · (kg · ℃)$^{-1}$)
EA	1.54	2 500	946
SMA	1.83	2 400	1 168
GA	1.30	2 500	942
UHPP-C	1.43	2 550	925
UHPP-S	1.49	2 480	910
UHPP-D	0.8	2 180	670
Steel	60	7 850	460

2.2.2 Mechanical response model

The temperature field model calculation results were incorporated into the mechanical models as field conditions, along with the bending moment stress state of the steel bridge deck, to analyze the mechanical response of SBDP during its service period. The bottom of the diaphragm was constrained for consolidation, and the longitudinal direction of SBDP was restricted from horizontal displacement. To ensure synchronous deformation, a rigid connection was implemented between the pavement and the steel bridge deck.

The vehicle loads were represented by a 0.189-m rectangular load with a tire pressure of 0.91 MPa, simulating a 30% overload scenario. In the longitudinal direction, considering the symmetry of the model, the initial load position of the vehicle load was set at the top of the transverse diaphragm and then moved longitudinally along the pavement to the midpoint between the two transverse diaphragms. Three typical positions were chosen in the transverse direction[13]. The material parameters used in this section are shown in Table 9.

Table 9 Material parameters of the finite element model

Pavement		UHPP-D	UHPP-S	UHPP-C	EA	GA	SMA	Steel
Elastic modulus/MPa	$T_{test} = 20$ ℃	500	870	980	1 000	535	800	210 000
	$T_{test} = 40$ ℃	340	550	650	700	229	470	210 000
	$T_{test} = 60$ ℃	270	430	470	500	195	350	210 000
Poisson's ratio		0.25	0.35	0.35	0.35	0.35	0.35	0.25
Linear expansion/10^{-5}		2.8	3.0	1.74	1.74	3.36	2.35	7.80

Note: T_{test} is the test temperature.

3 Results and Discussion

3.1 Anti-rutting performance under high temperature

The results of the rutting test under a high temperature are shown in Fig. 6. As illustrated in Fig. 6, the 70 ℃ dynamic stability of the UHPP composite structure decreased with an increase in the thickness of UHPP-D. This phenomenon could mainly be attributed to the design of UHPP-D, which incorporated a large pore structure ranging from 17% to 25%. With the increased thickness of UHPP-D, UHPP contained a greater number of pores, rendering it more susceptible to compression deformation under the load of vehicles. The varying degrees of dispersion in the results of each experimental group supported this observation. The dynamic stabilities of Groups 1, 2, and 3 reached 4 610, 4 950, and 6 190 times/mm, respectively. The rutting resistance of Groups 1 and 2 closely resembled that of GA + SMA, whereas Group 3 outperformed the latter, exhibiting a relative increase in dynamic stability of 20.4%. Additionally, Group 3 demonstrated a smaller degree of dispersion. This provides evidence that UHPP, with a thinner UHPP-D, could achieve superior high-temperature performance, aligning with the design goals of UHPP.

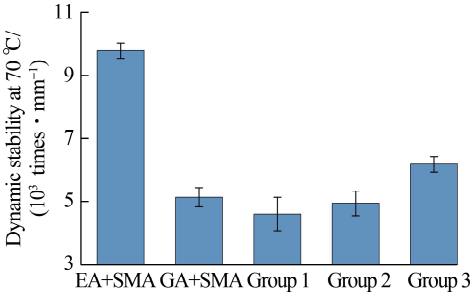

Fig. 6 Results of the rutting test under a high temperature

3.2 Antiskid performance during rainy weather

With reference to the summer rainfall in Guangzhou in 2020[12], friction coefficients of the composite structure under different rainfall conditions were obtained, as shown in Fig. 7.

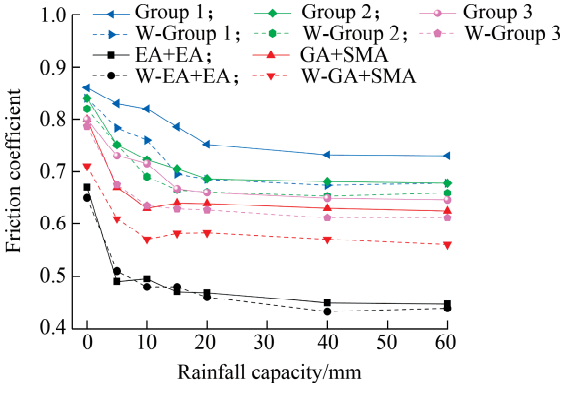

Fig. 7 Results of the antiskid test during rainy weather

The friction coefficient of the pavement surface reached its lowest point when the voids in SBDP became saturated with water. As shown in Fig. 7, the friction coefficient of all specimens gradually decreased and stabilized with increasing rainfall capacity. In the case of EA + EA, the surface voids reached saturation at approximately 5 mm of rainfall capacity, whereas this occurred at around 10 mm for GA + SMA. Group 1 of UHPP exhibited saturation at a rainfall capacity of over 20 mm, whereas Groups 2 and 3 experienced saturation at rainfall capacities of approximately 20 and 15 mm, respectively.

After the rutting test on the composite structure, varying degrees of reduction in the surface friction coefficient were observed. In the case of Group 1, which had a 2-cm UHPP-D, the reduction was most significant. This was mainly because the load applied during the rutting test damaged the pore structure, significantly reducing the drainage capacity. The difference in friction coefficients between Groups 2 and 3 was relatively minor. Even after the rutting test, their corresponding saturation rainfall capacity remained at approximately 10 to 15 mm, indicating that these two groups maintained enough surface antiskid performance. Combined with the results of the composite structure test, Group 3 was chosen to build the finite element model.

3.3 Temperature field of SBDP

To analyze the variations in the temperature fields of the three SBDPs, the results of temperature field calculations for pavement profiles were projected onto an *xy*-coordinate system that represents the time and depth of pavement. Integration was performed within each color region. The proportion of the pavement profile area within a specific temperature range, denoted as P_{ab}, relative to the overall temperature range of the pavement was computed as

$$P_{ab} = \frac{S_{ab}}{S_{\text{tot}}} \times 100\% \tag{7}$$

where S_{ab} represents the area of pavement profiles within the temperature range from a to b; S_{tot} represents the total area within the 24-h temperature range of the pavement. The results of the SBDP temperature field are depicted in Fig. 8.

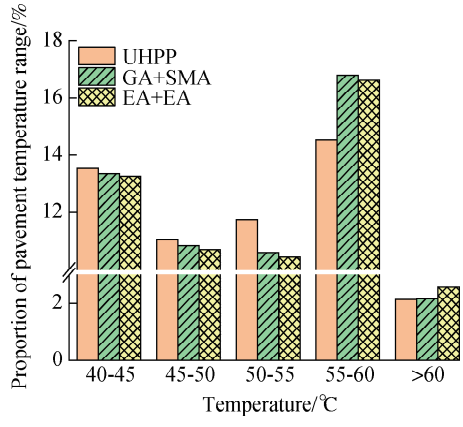

Fig. 8 Results of the SBDP temperature field

Combined with Fig. 8, in the temperature range above 40 ℃, the distribution trends of P_{ab} for the three SBDPs showed similarities. They all exhibited initially decreasing and then increasing trends, which finally decreased again. The area proportion of pavement profiles between 55 and 60 ℃ was the highest, followed by the 40-45 ℃ range. Meanwhile, the proportion of areas above 60 ℃ was the lowest. In the 55-60 ℃ range, P_{ab} of UHPP was significantly lower than those of the other two SBDPs, being 15.9% lower than that of GA + SMA and 14.7% lower than that of EA + EA. Overall, although UHPP reached a peak temperature of 62.9 ℃, it demonstrated a lower proportion of P_{ab} within the 55-60 ℃ range compared with the other two SBDPs. This suggests that the UHPP experienced fewer high-temperature conditions, which is advantageous for mitigating the potential for high-temperature deformation in asphalt mixtures.

3.4 Critical loading position

Tensile stress is a commonly used evaluation index to characterize the crack resistance of SBDP. The critical loading positions of vehicle loads on UHPP were analyzed initially. The results of surface tensile stresses for UHPP-D and UHPP-S were extracted, as shown in Figs. 9 and 10, respectively.

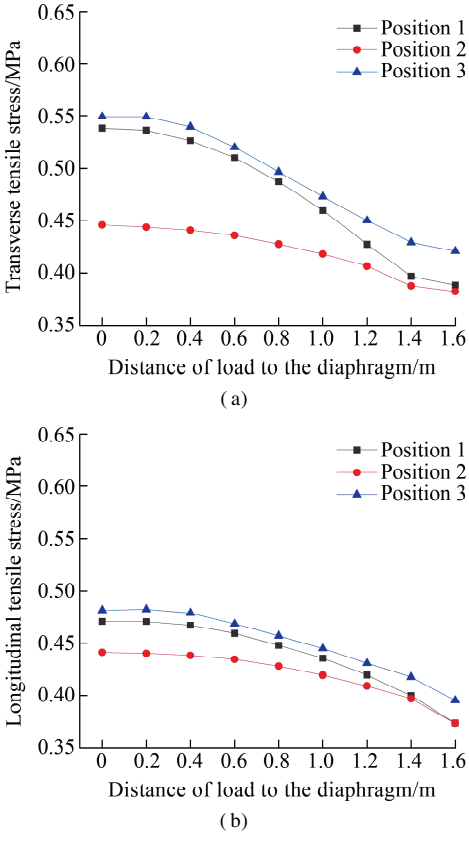

Fig. 9 Tensile stress on the top of UHPP-D under different load positions. (a) Transverse tensile stress; (b) Longitudinal tensile stress

As depicted in Fig. 9, the transverse tensile stress in UHPP-D was consistently slightly higher than the longitudinal tensile stress. Furthermore, as the distance from the transverse diaphragm increased, the magnitude of the tensile stress also decreased. Near the diaphragm, both the transverse and longitudinal tensile stresses in UHPP-D reached their maximum values. Following the application of three typical load positions in the transverse direction, position Ⅲ resulted in higher tensile stresses on the surface of UHPP-D compared with the other two positions. This indicates that the least favorable critical loading for UHPP-D was position Ⅲ near the top of the diaphragm.

As illustrated in Fig. 10, the surface tensile stress in UHPP-S gradually decreased with the increasing distance from the loading position and the transverse diaphragm, reaching its minimum value at the midpoint between adjacent transverse diaphragms. Under position Ⅲ loading, the peak transverse tensile stress was 0.644 MPa, whereas

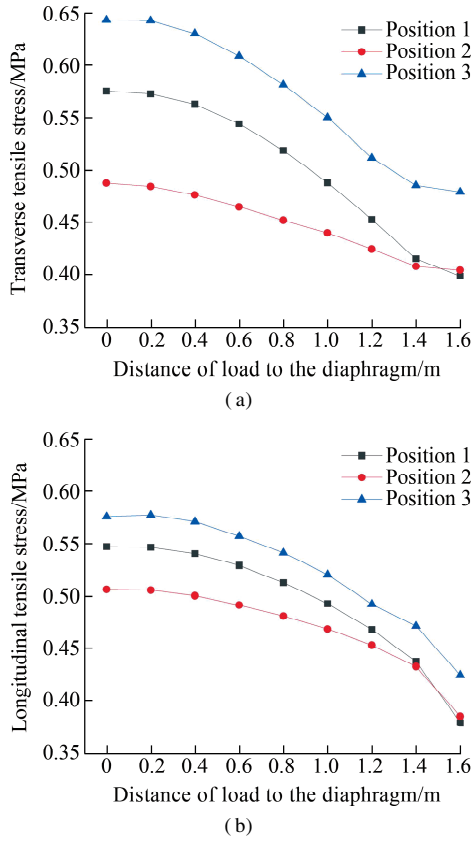

Fig. 10 Tensile stress on the top of UHPP-S under different load positions. (a) Transverse tensile stress; (b) Longitudinal tensile stress

the longitudinal tensile stress was 0.578 MPa.

The computed results indicated the presence of significant stress concentrations in the UHPP near the top of the transverse diaphragm. Meanwhile, the load in position Ⅲ represented the least favorable critical loading position.

3.5 Critical stress status

In this section, peak values of temperature-stress responses at unfavorable loading positions were extracted[14]. Considering that the control group of SBDPs (EA + EA and GA + SMA) involved in this article were both double-layer structures, lower and upper were used to refer to the upper and lower layers of these SBDPs, as depicted in Fig. 11.

As shown in Fig. 11, significant differences existed in the peak stresses among the three types of SBDPs. For instance, EA + EA followed a rigid design, resulting in a relatively high sensitivity of the stress response to temperature and deformation. The transverse and longitudinal tensile stress peaks in this SBDP both appeared in the upper layer, measuring 1.929 and 0.571 MPa, respectively. Furthermore, the rapid heat conduction of the EA mixture, coupled with expansion and contraction due to temperature effects, resulted in relatively high interlaminar shear stress. Meanwhile, GA + SMA represented a flexible SBDP, and the incorporation of composite modifiers

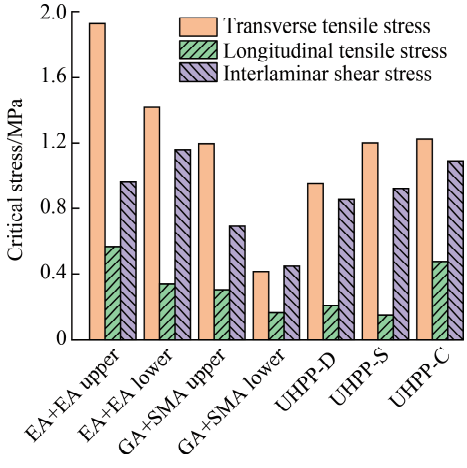

Fig. 11 Critical stress of SBDPs

maximized the viscoelastic properties of the asphalt, leading to relatively lower stress responses.

Regarding surface transverse and longitudinal tensile stresses, UHPP-D exhibited minimal differences from the other pavement layers. This was due to the thickness proportions and high modulus of UHPP-S and UHPP-C, which effectively distributed the effects of bridge bending and vehicle loading. Furthermore, transverse and longitudinal tensile stresses in UHPP-D and UHPP-S aligned with those in GA + SMA, indicating the absence of severe stress concentration in these two layers. However, UHPP-D, characterized by its high porosity design, notably had limited structural strength, making it more prone to cracking. Among the three layers of UHPP, UHPP-C experienced the highest surface tensile stress and interlaminar shear stress, primarily because of its design with a rigid base. The high structural strength and stiffness of epoxy resin mixed with gravel resulted in a firm bonding of UHPP to the steel bridge deck. Consequently, UHPP maintained a favorable overall stress state, with potential distress risks primarily concentrated in UHPP-C, necessitating strict control of the material properties of UHPP-C.

Given the aforementioned observations, the surface tensile stresses in the UHPP SBDP were evidently relatively low, but the interlaminar shear stress between UHPP-C and the steel bridge deck panel was relatively high. The main potential distress risks in UHPP were predominantly associated with UHPP-C, thus requiring strict control of its material properties. Additionally, measures such as incorporating interlayer gravel and optimizing adhesive layer quantities should be implemented to enhance the interlaminar shear resistance of UHPP-C.

4 Case Study

The Zhujiang Huangpu Bridge, constructed and opened to traffic in 2008, spans across the Pearl River in Guangdong Province, China, and serves as a pivotal regional transportation infrastructure. The region has an average annual temperature of 22 ℃, with summer highs reaching up to 43.7 ℃. Peak rainfall measurements scale up to 2 678.9 mm. Rainfall in the region is notably concentrated, with the rainy season accounting for 81% of the yearly total.

In 2014, because of the cumulative impact of prolonged heavy traffic, the SBDP of the Zhujiang Huangpu Bridge underwent significant refurbishment. After evaluating multiple remediation plans, UHPP was chosen as the primary rehabilitation strategy. In this project, a gravel layer was set between the UHPP-S and UHPP-D to enhance the shear resistance. After nearly nine years in service, no structural damages have been observed in the UHPP SBDP.

5 Conclusions

1) According to the RBFT concept, the lower pavement layer should possess outstanding crack resistance, whereas the upper layer should be constructed using more flexible and resilient materials. The UHPP proposed in this paper consisted of three layers: UHPP-C, UHPP-S, and UHPP-D. UHPP-C was made from epoxy resin and gravel. UHPP-S was reinforced with basalt fibers and polymer-modified asphalt. UHPP-D was a thin, porous layer and enhanced the rain-skid performance of SBDP.

2) Compared with the traditional GA + SMA, the highest improvement in dynamic stability of UHPP could reach up to 20.4%. Antiskid tests illustrated that UHPP-D effectively increased the friction coefficient between vehicles and the pavement surface during rainy conditions.

3) Notably, UHPP exhibited relatively higher shear stress, implying potential risks within the interlayer of SBDP. Incorporating interlayer gravel and optimizing adhesive layer quantities may be considered to ensure sufficient interlaminar shear resistance for the UHPP.

References

[1] Liu Y, Qian Z D, Hu H B, et al. Developing a skid resistance prediction model for newly built pavement: Application to a case study of steel bridge deck pavement [J]. *Road Materials and Pavement Design*, 2022, **23** (10): 2334 − 2352. DOI: 10.1080/14680629.2021.1972033.

[2] Jia X Y, Huang B S, Chen S J, et al. Comparative investigation into field performance of steel bridge deck asphalt overlay systems [J]. *KSCE Journal of Civil Engineering*, 2016, **20** (7): 2755 − 2764. DOI: 10.1007/s12205-016-0259-1.

[3] Bo W, Ren H S, Geng W, et al. Investigation of the environmental impacts of steel deck pavement based on life cycle assessment [J]. *Journal of Southeast University (English Edition)*, 2020, **36** (3): 334 − 340. DOI: 10.3969/j.issn.1003-7985.2020.03.012.

[4] Luo S, Lu Q, Qian Z D. Performance evaluation of epoxy modified open-graded porous asphalt concrete [J]. *Construction and Building Materials*, 2015, **76**: 97 − 102. DOI: 10.1016/j.conbuildmat.2014.11.057.

[5] Lu Q, Bors J. Alternate uses of epoxy asphalt on bridge decks and roadways[J]. *Construction and Building Materials*, 2015, **78**: 18 - 25. DOI: 10.1016/j.conbuildmat.2014.12.125.

[6] Zou G L, Zhang X N, Wu C. Evaluation of steel bridge deck MA mixture properties during construction[J]. *Journal of Marine Science and Technology*, 2015, **23**: 293 - 301. DOI: 10.6119/JMST-014-0327-2.

[7] Wang M, Xiao L, Hu D Y, et al. Rheological properties of gussasphalt mixture[J]. *Journal of Building Materials*, 2017, **20**(4): 630 - 634. DOI: 10.3969/j.issn.1007-9629.2017.04.023. (in Chinese)

[8] Chen L L, Qian Z D, Chen D X, et al. Feasibility evaluation of a long-life asphalt pavement for steel bridge deck[J]. *Advances in Civil Engineering*, 2020, **2020**: 1 - 8. DOI: 10.1155/2020/5890945.

[9] Yang L, Xue Y, Qian Z D, et al. Design and research on steel deck pavement structure of Jiujiang Yangtze River Bridge[J]. *Highway Engineering*, 2021, **46**(3): 79 - 85. DOI: 10.19782/j.cnki.1674-0610.2021.03.012. (in Chinese)

[10] Kainuma S, Jeong Y S, Ahn J H, et al. Behavior and stress of orthotropic deck with bulb rib by surface corrosion[J]. *Journal of Constructional Steel Research*, 2015, **113**: 135 - 145. DOI: 10.1016/j.jcsr.2015.05.014.

[11] Yan Z Y, Jin Z Y, Zhao X L, et al. Dynamic response of bridge deck pavement of three-span steel-concrete composite continuous beam under moving loads[J]. *Journal of Southeast University*, 2019, **49**(6): 1109 - 1115. DOI: 10.3969/j.issn.1001-0505.2019.06.013. (in Chinese)

[12] Li C Z, Cai Y P, Zhang J M, et al. On the mesoscale characteristics of hard rains in the Perl River Delta on May 31, 2020[J]. *Guangdong Meteorology*, 2021, **43**(6): 6 - 10. DOI: 10.3969/j.issn.1007-6190.2021.06.002. (in Chinese)

[13] Liu Y, Qian Z D, Zhang M. Fatigue damage analysis of epoxy asphalt pavement for steel bridges considering coupled effects of heavy load and temperature variations[J]. *Journal of Southeast University* (*English Edition*), 2017, **33**(4): 478 - 483. DOI: 10.3969/j.issn.1003-7985.2017.04.014.

[14] Chen X B, Xu L B, Luo R L, et al. Influence of longitudinal slope on the mechanical response of steel deck pavement[J]. *Journal of Southeast University* (*English Edition*), 2018, **34**(1): 71 - 77. DOI: 10.3969/j.issn.1003-7985.2018.01.011.

高温多雨地区 UHPP 钢桥面铺装设计与性能评估

钱振东[1] 张少锦[2] 闵一桐[1] 赵鑫元[1]

([1] 东南大学智能运输系统研究中心,南京 211189)

([2] 扬州大学建筑科学与工程学院,扬州 510000)

摘要:为提升钢桥面铺装在高温多雨地区的服役性能,结合工程实践总结了“下刚上柔”概念,提出了一种三层结构的超高性能铺装(UHPP);通过铺装复合结构试验评估了 UHPP 的高温抗车辙与雨天抗滑性能;利用温度场模型,就典型高温天气下各铺装内部温度分布情况展开分析,并通过温度-应力耦合模型,探究了 UHPP 铺装的关键荷位及应力响应特征. 分析结果表明:与传统的 GA + SMA 相比,UHPP 复合结构动态稳定性最高可提升 20.4%;即使经过循环载荷作用,与 2 种传统钢桥面铺装相比,UHPP 仍表现出更优越的表面抗滑性能;UHPP 的厚度组成对其抗车辙性能和抗滑性能有显著影响;UHPP 的拉应力相对较低,但剪应力水平较高,且 UHPP 与钢板间的剪应力最高,说明 UHPP 潜在病害风险主要存在于铺装层间. 根据工程实例,可考虑引入层间碎石并优化黏层用量,以确保 UHPP 具有足够的层间抗剪能力.

关键词:钢桥面铺装;高温环境;多雨天气;下刚上柔;温度场;复合结构

中图分类号:U419.6